Final inversion of the Midcontinent Rift during the Rigolet Phase of the Grenvillian Orogeny:

Eben B. Hodgin[1][†], Nicholas L. Swanson-Hysell[1], James M. DeGraff[2], Andrew R.C. Kylander-Clark[3], Mark D. Schmitz[4], Andrew C. Turner[1], Yiming Zhang[1], Daniel A. Stolper[1]

[1]Dept. of Earth and Planetary Science, University of California, Berkeley, CA, USA

[2]Dept. of Geological and Mining Engineering and Sciences, Michigan Technical University, Houghton, MI, USA

[3]Dept. of Earth and Planetary Science, University of California, Santa Barbara, CA, USA

[4]Dept. of Geosciences, Boise State University, Boise, ID, USA

[†]ebenblake@berkeley.edu

This data repository material includes:

1) Section DR1 consisting of:

    Detailed methods for LA-ICPMS and CA-ID-TIMS U-Pb zircon geochronology;

    Detailed methods for LA-ICP-MS U-Pb calcite geochronology;

    Detailed methods for calcite clumped isotope analysis;

2) Five supplementary tables:

SECTION DR1: DETAILED ANALYTICAL METHODS

Zircon Mineral Separation and Zircon Imaging

In the lab, detrital zircon rock samples were carefully scrubbed with a wire brush and cleaned with

compressed air prior to mineral separation. Zircon grains were separated from rock samples using

a sledgehammer, disc mill, 425 µm sieve, hydraulic gravitation separation via panning, methylene

iodide heavy liquid, and a Frantz magnetic separator at University of California Berkeley (UC

Berkeley). Zircons were annealed at 900ºC for >48 hours in a muffle furnace, mounted in epoxy,

and polished. At Boise State University (BSU), Cathodoluminescence (CL) images of zircons were

obtained with a JEOL JSM-300 SEM in combination with a Gatan MiniCL.

LA-ICPMS U-Pb Zircon Geochronology

At BSU, zircon was analyzed by laser ablation inductively coupled plasma mass spectrometry (LA-ICP-MS) using a ThermoElectron X-Series II quadrupole ICPMS and New Wave Research UP-213 Nd:YAG UV laser ablation system. Analytical protocols, standard materials, and data reduction software developed at BSU were used for acquisition and calibration of U-Pb dates and a suite of high field strength elements (HFSE) and rare earth elements (REE). Zircons were ablated with a laser spot 25 µm wide using fluence and pulse rates of 2.5 J/cm^2 and 10 Hz, respectively, during a 45 second analysis (15 second gas blank, 30 second ablation) excavating a pit ~25 µm deep. Ablated material was carried to the nebulizer flow of the plasma by a 1.2 L/min He gas stream. Total sweep duration is 950 ms, and quadrupole dwell times were 5 ms for Si and Zr, 40 ms for ^{202}Hg, ^{204}Pb, ^{208}Pb, ^{232}Th, and ^{238}U, 80 ms for ^{206}Pb, 200 ms for ^{49}Ti and ^{207}Pb, and 10 ms for all other HFSE and REE. Background count rates were obtained prior to each spot analysis and subtracted from the raw count rate for each analyte. For concentration calculations, background-subtracted count rates were internally normalized to ^{29}Si and calibrated with the primary standards NIST SRM-610 and -612 glasses. Ablation pits that intersected mineral inclusions were identified based on Ti and P excursions, and associated sweeps were discarded. U-Pb dates from these analyses were retained if U-Pb ratios appeared to have been unaffected by the inclusions. Mass 204 signals were typically indistinguishable from zero following subtraction of Hg backgrounds, and dates are thus reported without common Pb correction. The Ti-in-zircon thermometer was calculated using an average TiO_2 activity value of 0.8 in crustal rocks (Watson et al., 2006).

Zircon U-Pb data were collected in laser ablation experiments in November, 2020 and March, 2021. For U-Pb and $^{207}Pb/^{206}Pb$ dates, instrumental fractionation of the background-

subtracted ratios was corrected, and dates were calibrated with respect to interspersed measurements of standards and reference materials. The primary standard Plešovice zircon (Sláma et al., 2008) was used to monitor time-dependent instrumental fractionation based on two analyses for every 10 analyses of unknown zircon. Secondary standards were also analysed twice for every 10 unknowns, and a secondary correction was applied to the ^{206}Pb/^{238}U dates using Seiland (530 Ma), Zirconia (327 Ma), and FC1 (1096 Ma).

Radiogenic isotope ratio and age error propagation for all analyses do not include uncertainty contributions from counting statistics and background subtraction. These uncertainties are the local standard deviations of the polynomial fits to the interspersed primary standard measurements versus time for the time-dependent, relatively larger U-Pb fractionation factor, and the standard errors of the means of the consistently time-invariant and smaller ^{207}Pb/^{206}Pb fractionation factor. These uncertainties are 0.62–0.84% (2σ) for ^{206}Pb/^{238}U and 0.33–0.74% (2σ) for ^{207}Pb/^{206}Pb. Analyses with ^{207}Pb/^{206}Pb vs. ^{206}Pb/^{238}U discordance between -10 and +15% were interpreted and reported as concordant, and analyses outside of this range were interpreted and reported as discordant. Concordant and discordant U-Pb dates are differentiated in Concordia plots in Figure DR1. Only concordant U-Pb ^{207}Pb/^{206}Pb dates are plotted in age probability distributions using a kernel density of 18 Ma in Figure DR2 (Vermeesch, 2018). Errors on dates from individual analyses are reported at 2σ; all zircon LA-ICP-MS results are reported in Table DR1.

CA-ID-TIMS U-Pb Zircon Geochronology

Paired U-Pb detrital zircon dating was used to produce accurate and precise dates on rare populations of detrital zircons by combining two techniques: LA-ICP-MS to rapidly screen many detrital zircons followed by chemical abrasion–isotope dilution–thermal ionization mass

spectrometry (CA-ID-TIMS) on the youngest detrital zircons. We selected 19 detrital zircons with the youngest concordant LA-ICP-MS dates (~1050–950 Ma) for more accurate and precise CA-ID-TIMS dating. To test analytical reproducibility, five detrital zircons were broken into multiple fragments yielding a total of 25 CA-ID-TIMS analyses from 19 detrital zircons grains.

U-Pb dates were obtained by the CA-ID-TIMS method from analyses of single zircon grains or fragments of grains, modified after (Mattinson, 2005). Annealed zircon grains were selected from the epoxy mounts based on LA-ICP-MS data and CL images. Single grains or fragments were transferred to 3 ml Teflon PFA beakers, loaded into 300 µl Teflon PFA microcapsules with 120 µl of 29 M HF, placed in a large-capacity Parr vessel, and partially dissolved for 12 hours at 190°C.

The zircon grains or fragments were returned to 3 ml Teflon PFA beakers, HF removed, and rinsed in ultrapure H_2O, immersed in 3.5 M HNO_3, ultrasonically cleaned for one hour, and fluxed at 80°C for one hour. The HNO_3 was removed and grains or fragments were rinsed twice in ultrapure H_2O, then reloaded into Teflon PFA and spiked with Boise State BSU1B tracer solution with a calibration of $^{235}U/^{205}Pb = 77.93$ and $^{233}U/^{235}U = 1.007066$. Zircon was dissolved in Parr vessels in 120 µl of 29 M HF at 220°C for 48 hours, dried to fluorides, and re-dissolved in 6 M HCl at 180°C overnight. Uranium and Pb were separated from the zircon matrix using an HCl-based anion-exchange chromatographic procedure (Krogh, 1973), eluted together, and dried with 2 µl of 0.05 N H_3PO_4.

Uranium and Pb were loaded on a single outgassed Re filament in 5 µl of a silica-gel/phosphoric acid mixture (Gerstenberger and Haase, 1997), and U and Pb isotopic measurements made on a GV Isoprobe-T multicollector thermal ionization mass spectrometer equipped with an ion-counting Daly detector. Pb isotopes for analyses with smaller amounts of

radiogenic Pb were measured by peak-jumping all isotopes on the Daly detector for 150 cycles, and corrected for 0.16 ± 0.06/a.m.u. (2σ) mass fractionation. Pb isotopes for analyses with larger amounts of radiogenic Pb were measured by a Faraday-Daly routine that cycles 150-200 times between placing mass 204 in the axial Daly collector and masses 205-208 on the H1-H4 Faraday detectors to placing mass 205 in the axial Daly and masses 206-208 in the H1-H3 Faradays, providing real-time Daly gain correction. These results were corrected for $0.10 \pm 0.06\%$/a.m.u. (2σ) mass fractionation. Transitory isobaric interferences due to high-molecular weight organics, particularly on ^{204}Pb and ^{207}Pb, disappeared within approximately 30 cycles. The ionization efficiency of each Pb isotope averaged 10^4 cps/pg. Linearity (to $\geq 1.4 \times 10^6$ cps) and the associated deadtime correction of the Daly detector were monitored by repeated analyses of NBS982. Uranium was analyzed as UO_2^+ ions in static Faraday mode on 10^{11} or 10^{12} ohm resistors for 200-300 cycles, and corrected for isobaric interference of ^{233}U^{18}O^{16}O on ^{235}U^{16}O^{16}O with an ^{18}O/^{16}O of 0.00206. Ionization efficiency averaged 20 mV/ng of each U isotope. Uranium mass fractionation was corrected using the known ^{233}U/^{235}U ratio of the tracer solutions.

CA-ID-TIMS U-Pb dates and uncertainties were calculated using the algorithms of (Schmitz and Schoene, 2007), and U decay constants recommended by Hiess et al. (2012). ^{206}Pb/^{238}U ratios and dates were corrected for initial ^{230}Th disequilibrium using a Th/U[magma] = 3.0 ± 0.3, resulting in an increase in the ^{206}Pb/^{238}U dates of ~0.09 Ma. All common Pb in analyses was attributed to laboratory blank and subtracted based on the measured laboratory Pb isotopic composition and associated uncertainty. Uranium blanks were estimated at 0.013 pg.

CA-ID-TIMS weighted mean ^{206}Pb/^{238}U dates were calculated from equivalent dates (pof >0.05) using Isoplot 3.0 (Ludwig, 2003). Errors on the weighted mean dates are given as $\pm$ x / y / z, where x is the internal error based on analytical uncertainties only, including counting statistics,

subtraction of tracer solution, and blank and initial common Pb subtraction, y includes the tracer calibration uncertainty propagated in quadrature, and z includes the ^{238}U decay constant uncertainty propagated in quadrature. Internal errors should be considered when comparing our dates with ^{206}Pb/^{238}U dates from other laboratories that used the same EARTHTIME tracer solution or a tracer solution that was cross-calibrated using EARTHTIME gravimetric standards. Errors including the uncertainty in the tracer calibration should be considered when comparing our dates with those derived from other geochronological methods using the U-Pb decay scheme (for example LA-ICP-MS). Errors including uncertainties in the tracer calibration and ^{238}U decay constant (Hiess et al., 2012) should be considered when comparing our dates with those derived from other decay schemes (for example ^{40}Ar/^{39}Ar, ^{187}Re-^{187}Os). Errors for weighted mean dates and dates from individual grains are given at 2σ and shown in Table DR2.

Calcite U-Pb Geochronology

At the University of California Santa Barbara (UCSB), calcite U-Pb geochronology was carried out by LA-ICP-MS using a Photon Machines Excite 193 nm Excimer laser coupled with a Nu Plasma 3D MC-ICPMS, following the methods of Kylander-Clark (2020). Laser experiments were carried out September 28th and 29th, 2020. For each analysis, a ~110 μm spot size was ablated at 10 Hz for 15 seconds with a 20 second washout, following 2 shots of pre-ablation, using a fluence of ~1 J/cm^2. Data was reduced in two stages: 1) data was first reduced using NIST614 to correct the ^{207}Pb/^{206}Pb ratio and for instrument drift in the ^{206}Pb/^{238}U ratio using Iolite v3.5 (Paton et al., 2010); and 2) the ^{206}Pb/^{238}U ratios of NIST614-corrected data were corrected such that the reference material WC-1 (Roberts et al., 2017) yielded the accepted value of 254 Ma. Secondary reference materials ASH-15 (2.96 Ma; Nuriel et al., 2020) and Duff Brown Tank (64 Ma; Hill et

al., 2016) yielded ages of 2.89 ± 0.15 Ma (n = 11) and 65.7 ± 0.9 Ma (n = 8), respectively, consistent with their accepted values. Isochrons were calculated using IsoplotR (Vermeesch, 2018) using model 3 algorithm, in which the overdispersion factor, ω, is interpreted as geological scatter. All data from sample LLB2 (96 of 96 analyses) were included in the isochron age calculation (Fig. 3). All data except four outliers (93 of 97 analyses) were included in the isochron age calculation for LLB6 (Fig. DR3).

Calcite stable isotope geochemistry and thermometry: Measurement of clumped, carbon, and oxygen isotopic measurements

Isotopic measurements of $\delta^{13}C$, $\delta^{18}O$, and Δ_{47} values were performed in the Department of Earth and Planetary Science at UC Berkeley. Measured values for the samples are given in Table DR5, sheet 1 while standards are given in Table DR5, sheet 2. Samples were converted to CO_2 and purified using an automated carbonate extraction line designed after that described in Passey et al. (2010). In brief, ~8 mg of sample was digested in 104% phosphoric acid at 90°C and the evolved CO_2 purified cryogenically and using a gas chromatograph before introduction into a Thermo 253+ isotope ratio mass spectrometer (IRMS). Isotopic ratios were measured following procedures outlined in Eiler and Schauble (2004), Huntington et al. (2009), and Dennis et al. (2011) using the ^{17}O correction outlined in Brand et al. (2010). Measured Δ_{47} are background corrected using a mass 47.5 cup as described in Fiebig et al. (2019).

$\delta^{13}C_{carb}$ and $\delta^{18}O_{carb}$ values are given relative to the VPDB scales. Initial values are first reported relative to a calibrated reference gas standard from OzTech Inc assuming an oxygen

isotope acid digestion fractionation factor of 1.00821 from Swart et al. (1991). Samples were then corrected to the VPDB scale based on the values of ETH standards given in Bernasconi et al. (2018). Accuracy was evaluated by measuring the IAEA-603 international calcite standard (n = 10). Average measured values agree with declared values to within 0.02‰ for $\delta^{18}O$ and 0.01‰ for $\delta^{13}C$ following these corrections.

Final Δ_{47} values are placed into the so-called ETH reference frame as follows. First, samples are placed into the absolute reference frame by measured samples of CO_2 equilibrated either at 25 °C with water or heated at 1000 °C following the methodology given in Dennis et al. (2011). In doing this, residual dependences of measured Δ_{47} values on bulk isotopic composition (as given by $\delta 47$) are removed. Slopes are <0.001‰ in all cases. Following this, measurements are corrected to agreed-upon Δ_{47} values of the ETH 1, 2, 3, and 4 standards given in Bernasconi et al. (2021) based on the values given in Table 1 of that study. To do this, we use the slope and intercept of measured vs. accepted values of these standards to correct samples into this reference frame. Values we measured for the ETH standards prior to this final correction are given in Table DR5, sheet 2. After correction, we then calculate temperature from Δ_{47} using the regression from Anderson et al. (2021).

Sample analyses were replicated three times each over the course of one analytical session between September and December 2020. Accuracy and external reproducibly was evaluated as follows. Throughout the analytical session, we measured two in-house standards: a marble termed CAR1 (n = 34 during the session presented here) and a travertine (TRV1; n = 32) and an international reference standard, IAEA-603 (n = 10). Average Δ_{47}, $\delta^{18}O_{carb}$, and $\delta^{13}C_{carb}$ and standard deviation of all standards measured in this session are given in Table DR5, sheet 2. For CAR1, TRV1, and IAEA-603 standards, we provide values following correction to the ETH

declared values. As discussed above regarding the ETH standards, we provide values measured following all corrections except for final correction to the declared values of the ETH standards.

External reproducibility was evaluated via the replicate measurement of the CAR1, TRV1, and IAEA-603 standards. Standard deviations ($\pm 1\sigma$) for Δ_{47}, $\delta^{18}O$, and $\delta^{13}C$ were <0.010, 0.08, and 0.09‰ respectively. Accuracy was evaluated as follows: In Bernasconi et al. (2021), the authors report a $\Delta_{47(I\text{-}CDES)}$ (in the 90°C reference frame) for IAEA-C1, a Carrara marble standard, as 0.3018 ± 0.0013 (1 s.e.). As mentioned above, we also measure IAEA-603, a different Carrara marble standard from the IAEA. After correction to ETH standards, we report a Δ_{47} of 0.3043 ± 0.0031 (1 s.e.). Thus, these Carrara marbles, though different, agree in Δ_{47} values to within $\pm$ 1 s.e.

DATA REPOSITORY MATERIAL TABLE AND FIGURE CAPTIONS

Table DR1. LA-ICP-MS U-Pb zircon age and trace element data

Table DR2. CA-ID-TIMS U-Pb zircon age data

Table DR3. Comparison of LA-ICP-MS and CA-ID-TIMS U-Pb zircon dates from the youngest Jacobsville Fm detrital zircons

Table DR4. LA-ICP-MS U-Pb calcite age data

Table DR5: Carbonate Clumped Isotope data include the following: ETH-corrected values of Δ_{47}, Δ_{47}-based temperature calculations, $\delta^{18}O_{carb}$ (VPDB), $\delta^{13}C_{carb}$ (VPDB), and $\delta^{18}O_{carb}$

(VSMOW) for calcite samples and standards. VPDB = Vienna Pee Dee Belemnite. VSMOW = Vienna Standard Mean Ocean Water, calculated following Watkins et al. (2014).

Figure DR1. Concordia plots of LA-ICP-MS U-Pb detrital zircon data from the Jacobsville Sandstone. A) Sample AF1-29.3, Agate Falls, 237 concordant analyses out of 273 total analyses; B) BSC1-92.5, Snake Creek, 106 concordant analyses out of 136 total analyses; C) NW1-61.5, Natural Wall, 200 concordant analyses out of 224 total analyses; D) SC18-1, Sandstone Creek, 338 concordant analyses out of 378 total analyses. Ellipses of concordant analyses (-10 to +15% discordance) are light blue. Ellipses of discordant analyses (<-10 or >+15% discordance) are white. Discordance is calculated as the percent difference in $^{206}Pb/^{238}U$ vs. $^{207}Pb/^{206}Pb$ dates.

Figure DR2. Kernel Density plots of concordant LA-ICP-MS U-Pb detrital zircon data from four samples of Jacobsville Sandstone in northern Michigan (see Figure 1 and main text for sample locations). A) Sample AF1-29.3 at Agate Falls, 237 concordant analyses; B) BSC1-92.5 at Snake Creek, 106 concordant analyses; C) NW1-61.5 at Natural Wall, 200 concordant analyses; D) SC18-1 at Sandstone Creek, 338 concordant analyses. $^{207}Pb/^{206}Pb$ dates are plotted using a kernel density of 18 Ma (Vermeesch, 2018).

Figure DR3. Tera-Wasserburg plot of LA-ICP-MS U-Pb data from calcite sample LLB6 from the Keweenaw Fault at Lac Labelle. Lower intercept date of 1020.2 ± 98.8 Ma (2σ) determined from 93 of 97 LA-ICPMS analyses with unanchored upper intercept that gives an initial $^{207}Pb/^{206}Pb$ composition of 0.8494 ± 0.008 (2σ). Lower intercept determined using Model 3 dischord using IsoplotR (Vermeesch, 2018).
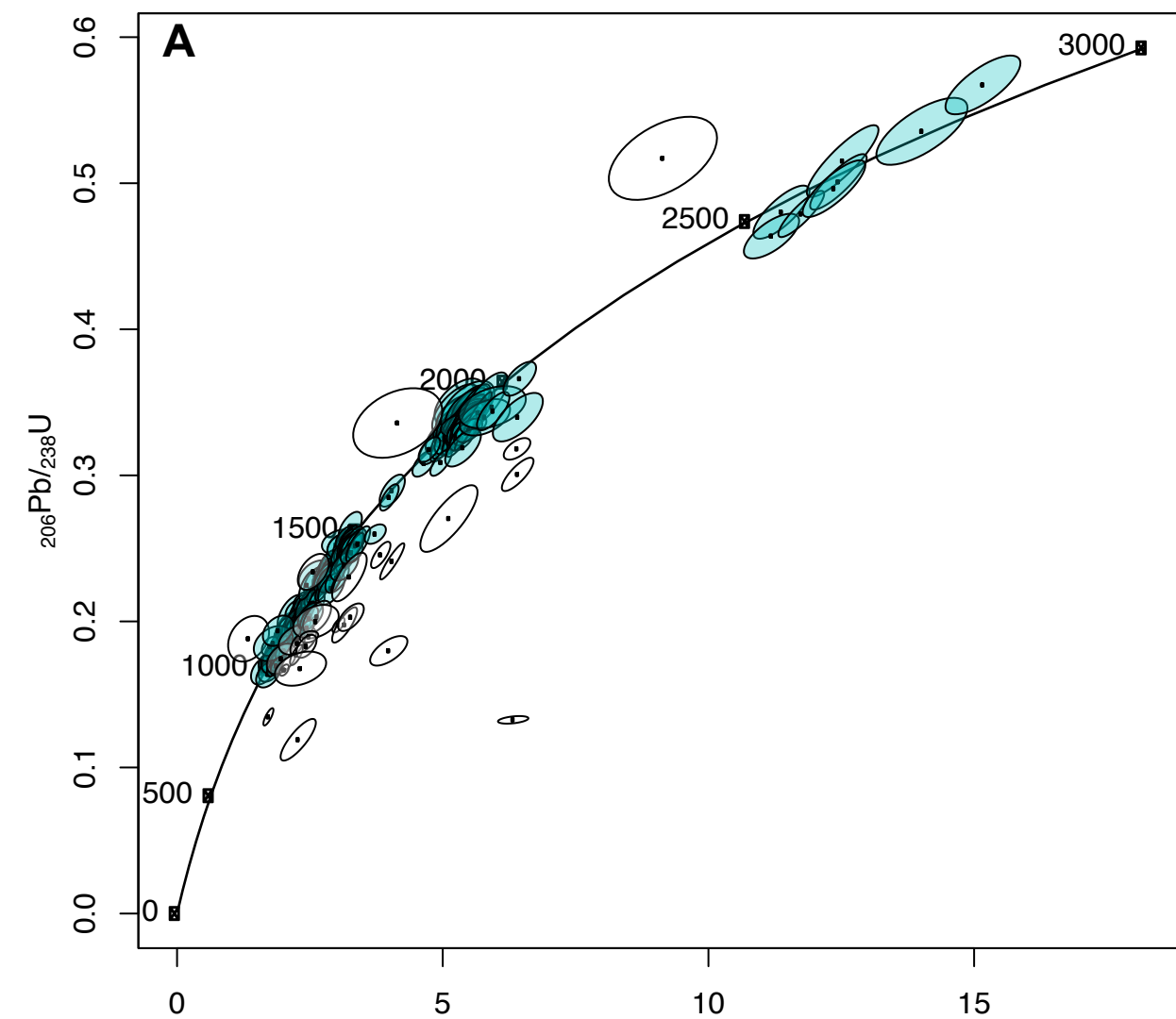
REFERENCES CITED

Anderson N. T., Kelson J. R., Kele S., Daëron M., Bonifacie M., Horita J., Mackey T. J., John C. M., Kluge T., Petschnig P., Jost A. B., Huntington K. W., Bernasconi S. M., and Bergmann K. D, 2021, A Unified Clumped Isotope Thermometer Calibration (0.5–1,100°C) Using Carbonate-Based Standardization. *Geophys. Res. Lett.* 48, e2020GL092069.

Bernasconi S. M., Müller I. A., Bergmann K. D., Breitenbach S. F. M., Fernandez A., Hodell D. A., Jaggi M., Meckler A. N., Millan I., and Ziegler M, 2018, Reducing Uncertainties in Carbonate Clumped Isotope Analysis Through Consistent Carbonate-Based Standardization. *Geochem. Geophys. Geosystems* 19, 2895–2914.

Bernasconi S. M., Daëron M., Bergmann K. D., Bonifacie M., Meckler A. N., Affek H. P., Anderson N., Bajnai D., Barkan E., Beverly E., Blamart D., Burgener L., Calmels D., Chaduteau C., Clog M., Davidheiser-Kroll B., Davies A., Dux F., Eiler J., Elliott B., Fetrow A. C., Fiebig J., Goldberg S., Hermoso M., Huntington K. W., Hyland E., Ingalls M., Jaggi M., John C. M., Jost A. B., Katz S., Kelson J., Kluge T., Kocken I. J., Laskar A., Leutert T. J., Liang D., Lucarelli J., Mackey T. J., Mangenot X., Meinicke N., Modestou S. E., Müller I. A., Murray S., Neary A., Packard N., Passey B. H., Pelletier E., Petersen S., Piasecki A., Schauer A., Snell K. E., Swart P. K., Tripati A., Upadhyay D., Vennemann T., Winkelstern I., Yarian D., Yoshida N., Zhang N. and Ziegler M., 2021, InterCarb: A community effort to improve inter-laboratory standardization of the carbonate clumped isotope thermometer using carbonate standards, *Geochem. Geophys. Geosystems* n/a, e2020GC009588.

Brand W. A., Assonov S. S. and Coplen T. B., 2010, Correction for the 17O interference in δ(13C) measurements when analyzing CO2 with stable isotope mass spectrometry (IUPAC Technical Report). *Pure Appl. Chem.* 82, 1719–1733.

Dennis K. J., Affek H. P., Passey B. H., Schrag D. P. and Eiler J. M., 2011, Defining an absolute reference frame for 'clumped' isotope studies of CO2. *Geochim. Cosmochim. Acta* 75, 7117–7131.

Eiler J. M. and Schauble E. (2004) 18O13C16O in Earth's atmosphere. *Geochim. Cosmochim. Acta* 68, 4767–4777.

Fiebig J., Bajnai D., Löffler N., Methner K., Krsnik E., Mulch A. and Hofmann S. (2019) Combined high-precision Δ48 and Δ47 analysis of carbonates. *Chem. Geol.* 522, 186–191.

Gerstenberger, H., and Haase, G., 1997, A highly effective emitter substance for mass spectrometric Pb isotope ratio determinations: Chemical Geology, v. 136, p. 309–312, doi:10.1016/S0009-2541(96)00033-2.
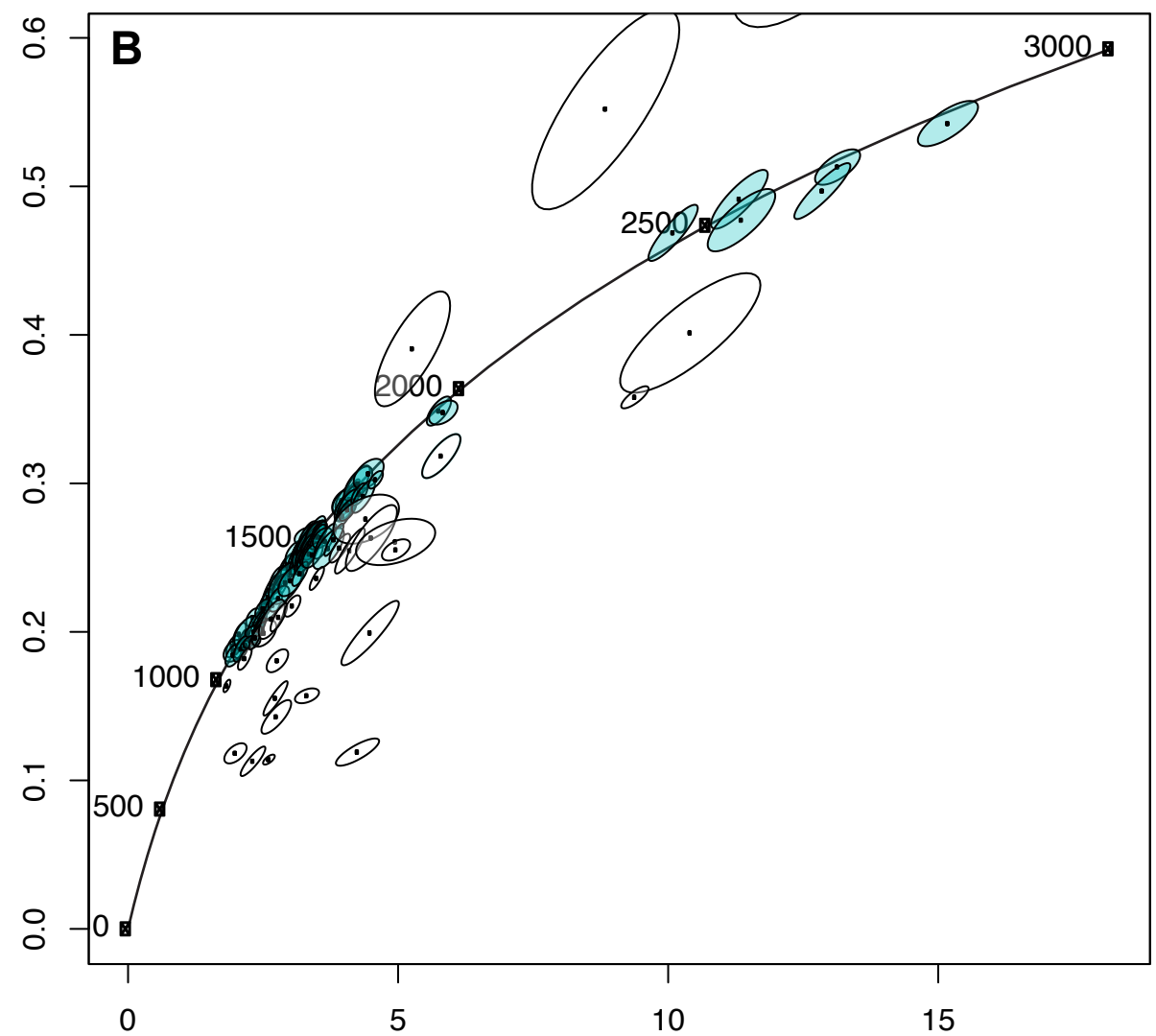
Hiess, J., Condon, D.J., McLean, N., and Noble, S.R., 2012. 238U/235U systematics in terrestrial uranium-bearing minerals. Science, v. 335, no. 6076, p. 1610–1614.

Hill, C. A., Polyak, V. J., Asmerom, Y., and P. Provencio, P. C. T. C., 2016, Constraints on a Late Cretaceous uplift, denudation, and incision of the Grand Canyon region, southwestern Colorado Plateau, USA, from U-Pb dating of lacustrine limestone: Tectonics, v. 35, p. 896–906, 10.1002/2016tc004166.

Huntington K. W., Eiler J. M., Affek H. P., Guo W., Bonifacie M., Yeung L. Y., Thiagarajan N., Passey B., Tripati A., Daëron M. and Came R. (2009) Methods and limitations of 'clumped' CO2 isotope (Δ47) analysis by gas-source isotope ratio mass spectrometry. *J. Mass Spectrom.* 44, 1318–1329.

Jackson, S.E., Pearson, N.J., Griffin, W.L., and Belousova, E.A., 2004, The application of laser ablation-inductively coupled plasma-mass spectrometry to in situ U-Pb zircon geochronology: Chemical Geology, v. 211, p. 47–69, doi:10.1016/j.chemgeo.2004.06.017.

Krogh, T.E., 1973, A low-contamination method for hydrothermal decomposition of zircon and extraction of U and Pb for isotopic age determinations: Geochimica et Cosmochimica Acta, v. 37, p. 485–494, doi:10.1016/0016-7037(73)90213-5.

Kylander-Clark, A.R.C., Hacker, B.R., and Cottle, J.M., 2013, Laser-ablation split-stream ICP petrochronology: Chemical Geology, v. 345, p. 99–112, doi:10.1016/j.chemgeo.2013.02.019.

Kylander-Clark, A.R., 2020, Expanding the limits of laser-ablation U–Pb calcite geochronology: Geochronology, v. 2, no. 2, p. 343–354.

Ludwig, K.R., 2003, User's manual for IsoPlot 3.0. A Geochronological Toolkit for Microsoft Excel: Berkeley Geochronology Center Special Publication, v. 4, p. 70.

Mattinson, J.M., 2005, Zircon U-Pb chemical abrasion ("CA-TIMS") method: Combined annealing and multi-step partial dissolution analysis for improved precision and accuracy of zircon ages: Chemical Geology, v. 220, p. 47–66, doi:10.1016/j.chemgeo.2005.03.011.

Nuriel, P., Wotzlaw, J.-F., Stremtan, C., Vaks, A., and Kylander-Clark, A. R., 2020, The use of ASH15 flowstone as matrix-matched standard for laser-ablation geochronology of calcite: Geochronology Discussions, p. 1–26. https://doi.org/10.5194/gchron-2020-22.

Odin, G., Montanari, A., Deino, A., Drake, R., Guise, P., Kreuzer, H., and Rex, D, 1991, Reliability of volcano-sedimentary biotite ages across the Eocene-Oligocene boundary (Apennines, Italy): Chemical Geology, v. 86, p. 203–224.

Passey B. H., Levin N. E., Cerling T. E., Brown F. H. and Eiler J. M. (2010) High-temperature environments of human evolution in East Africa based on bond ordering in paleosol carbonates. *Proc. Natl. Acad. Sci.* 107, 11245–11249.

Paton, C., Woodhead, J.D., Hellstrom, J.C., Hergt, J.M., Greig, A., and Maas, R., 2010, Improved laser ablation U-Pb zircon geochronology through robust downhole fractionation correction: Geochemistry, Geophysics, Geosystems, v. 11, no. 3, p. 1–36, doi:10.1029/2009GC002618.

Roberts, N. M. W., Rasbury, E. T., Parrish, R. R., Smith, C. J., Horstwood, M. S. A., and Condon, D. J., 2017, A calcite reference material for LA-ICP-MS U-Pb geochronology: Geochemistry Geophysics Geosystems, v. 18, p 2807–2814, 10.1002/2016GC006784,.

Schmitz, M.D., and Schoene, B., 2007, Derivation of isotope ratios, errors, and error correlations for U-Pb geochronology using 205Pb-235U-(233U)-spiked isotope dilution thermal ionization mass spectrometric data: Geochemistry, Geophysics, Geosystems, v. 8, no. 8, p. 1–20, doi:10.1029/2006GC001492.

Sláma, J., Košler, J., Condon, D.J., Crowley, J.L., Gerdes, A., Hanchar, J.M., Horstwood, M.S., Morris, G.A., Nasdala, L., Norberg, N., and Schaltegger, U., 2008, Plešovice zircon - A new natural reference material for U-Pb and Hf isotopic microanalysis: Chemical Geology, v. 249, p. 1–35, doi:10.1016/j.chemgeo.2007.11.005.

Swart P. K., Burns S. J. and Leder J. J. (1991) Fractionation of the stable isotopes of oxygen and carbon in carbon dioxide during the reaction of calcite with phosphoric acid as a function of temperature and technique. Chem. Geol. Isot. Geosci. Sect. 86, 89–96.

Vermeesch, P., 2018, IsoplotR: A free and open toolbox for geochronology: Geoscience Frontiers, v. 9, p. 1479–1493, doi:10.1016/j.gsf.2018.04.001.

Watkins, J.M., Hunt, J.D., Ryerson, F.J., and DePaolo, D.J., 2014, The influence of temperature, pH, and growth rate on the δ18O composition of inorganically precipitated calcite: Earth and Planetary Science Letters, v. 404, p. 332–343.

Watson, E.B., Wark, D.A., and Thomas, J.B., 2006, Crystallization thermometers for zircon and rutile: Contributions to Mineralogy and Petrology, v. 151, no. 4, p. 413–433, doi:10.1007/s00410-006-0068-5.

Wiedenbeck, M., Allé, P., Corfu, F., Griffin, W.L., Meier, F., Oberli, F., von Quadt, A., Roddick, J.C., and Spiegel, W., 1995, Three natural zircon standards for U-Th-Pb, Lu-Hf, trace element and REE analyses: Geostandards Newsletter, v. 19, p. 1–23.
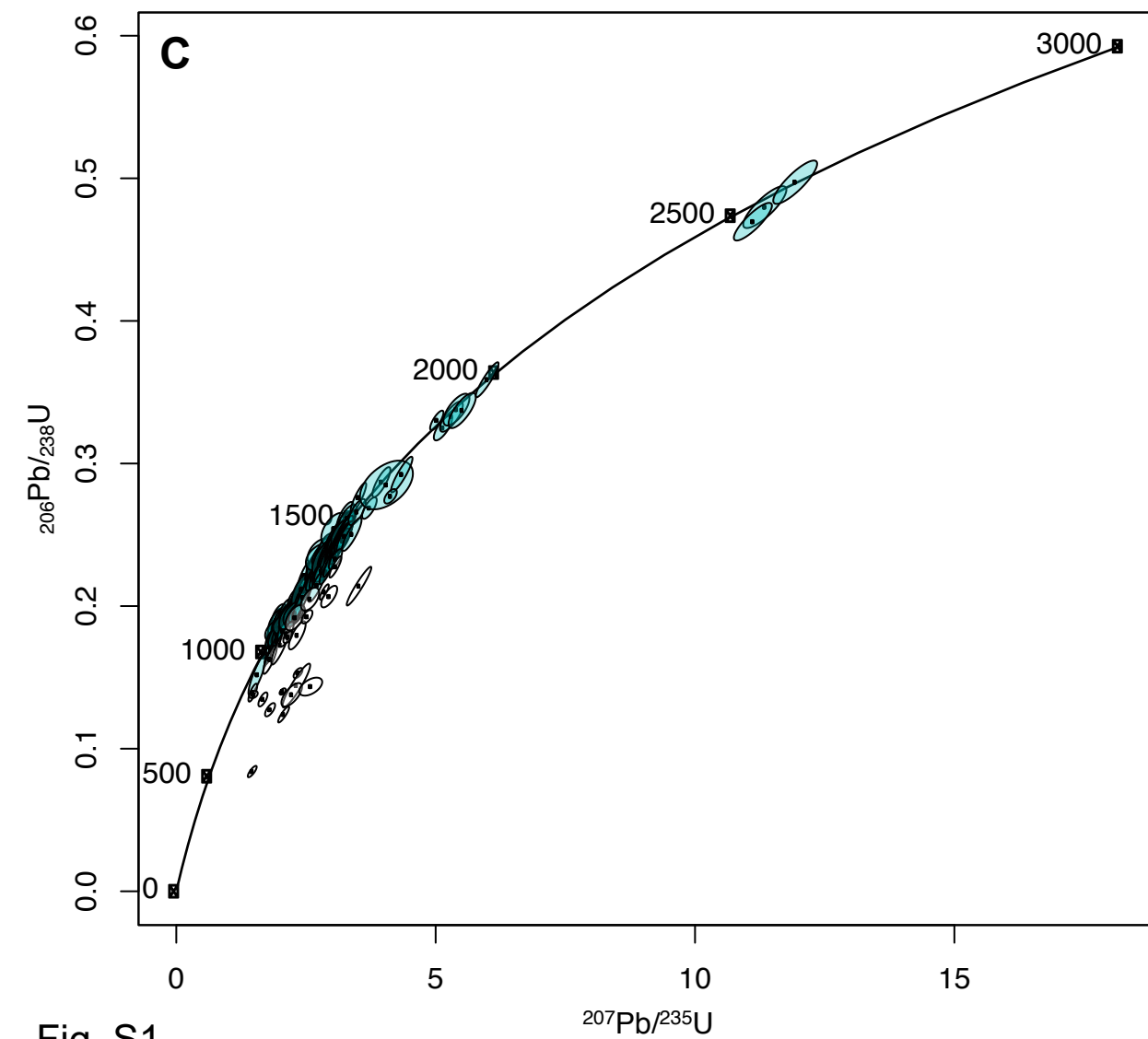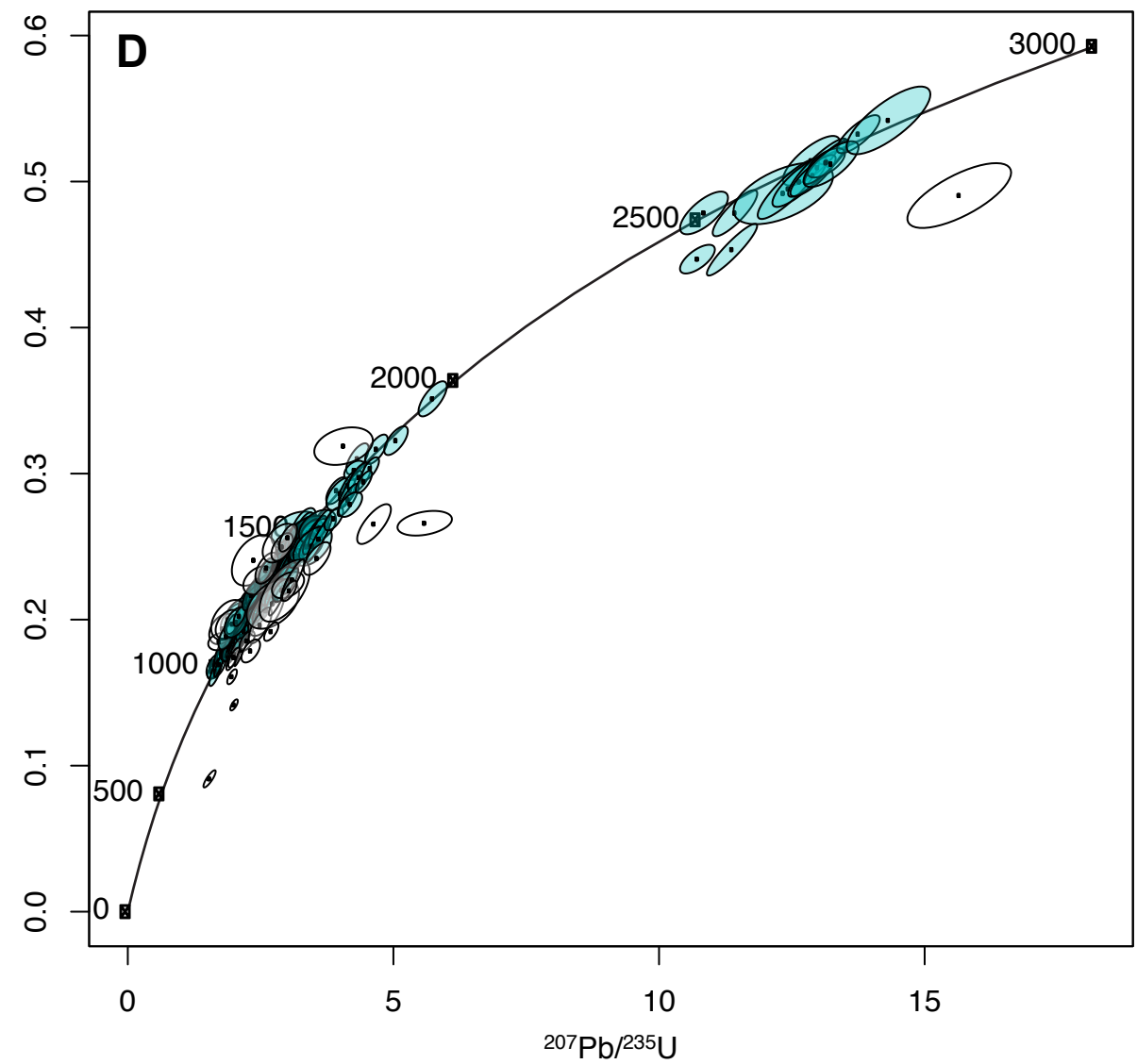
Fig. S1

A — AF1-29.3

B — BSC1-92.5

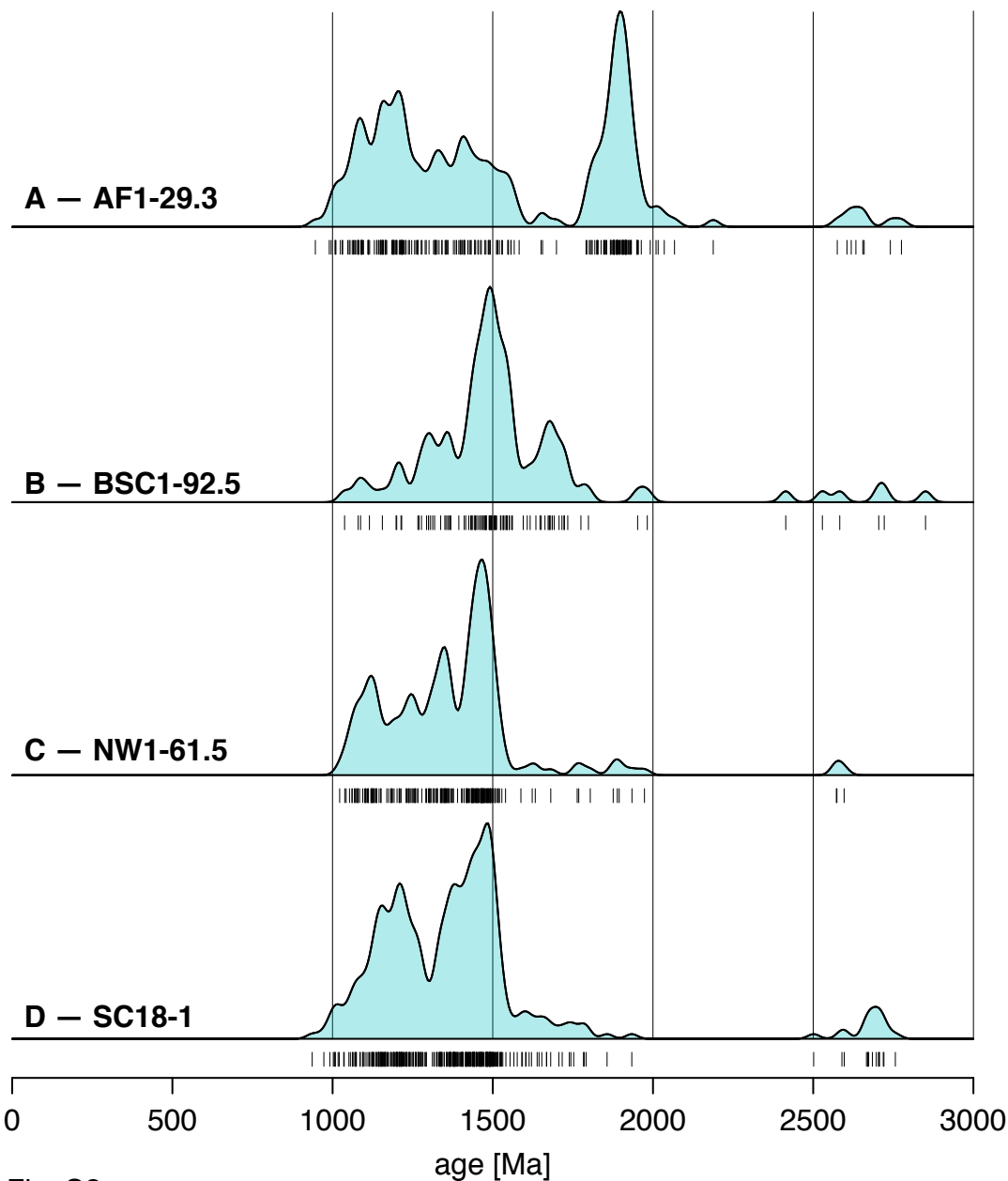C — NW1-61.5

D — SC18-1

age [Ma]

Fig. S2

1020.2 ± 98.8 Ma
MSWD = 1.2

5000

4000

3000

2000

$^{207}Pb/^{206}Pb$

$^{238}U/^{206}Pb$

Fig. S3